Applied Surface Science 611 (2023) 155436

Contents lists available at ScienceDirect

Applied Surface Science

journal homepage: www.elsevier.com/locate/apsusc

Full length article

Electronic structure of Bi nanolines on InAs(100)

Dhani Nafday [a], Christine Richter [b,c], Olivier Heckmann [b,c], Weimin Wang [d], Jean-Michel Mariot [e], Uros Djukic [b], Ivana Vobornik [f], Patrick Lefevre [g], Amina Taleb-Ibrahimi [g], Françoıs Bertran [g], Julien Rault [g], Laurent Nicolaï [h], Chin Shen Ong [i], Patrik Thunström [i], Karol Hricovini [b,c], Ján Minár [h], Igor Di Marco [a,i,j,*]

[a] Asia Pacific Center for Theoretical Physics, Pohang, Gyeonbuk 790-784, Republic of Korea
[b] Laboratoire de Physique des Matériaux et des Surfaces, CY Cergy Paris Université, 5 mail Gay-Lussac, 95031 Cergy-Pontoise, France
[c] Université Paris-Saclay, CEA, CNRS, LIDYL, 91191 Gif-sur-Yvette, France
[d] MAX IV Laboratory, Lund University, P.O. Box 118, 22100 Lund, Sweden
[e] Sorbonne Université, CNRS, Laboratoire de Chimie Physique–Matière et Rayonnement, 4 place Jussieu, 75252 Paris Cedex 05, France
[f] Istituto Officina dei Materiali, TASC Laboratory, CNR, Area Science Park-Basovizza, Strada Statale 14, km 163.5, 34149 Trieste, Italy
[g] Synchrotron SOLEIL, L'Orme des Merisiers, Départementale 128, 91190 Saint-Aubin, France
[h] New Technologies-Research Center, University of West Bohemia, 30100 Plzeň, Czech Republic
[i] Department of Physics and Astronomy, Uppsala University, P.O. Box 516, 75120 Uppsala, Sweden
[j] Department of Physics, Pohang University of Science and Technology, Pohang, Gyeonbuk 790-784, Republic of Korea

ARTICLE INFO

Keywords:
Bi nanolines
Self-assembly
Photoemission spectroscopy
InAs surface
Density-functional theory

ABSTRACT

Self-assembled nanolines are attractive to build the technological devices of next generation, but characterizing their electronic properties is often difficult to achieve. In this work we employ angle-resolved photoemission spectroscopy and density functional theory to clarify the electronic structure exhibited by self-assembled Bi nanolines grown on the InAs(100) surface. A surface resonance associated to the reconstructed $\zeta(4 \times 2)$ surface is visible in the photoemission spectra before and after the formation of the Bi nanolines. This demonstrates that Bi deposition does not necessarily drive a transition to an unreconstructed surface in the substrate, which is contrary to what was reported in previous studies. In addition, experiment and theory show the presence of a flat band located in the band gap of InAs, just above the valence band maximum. This flat band is associated to the Bi nanolines and possesses a strong orbital character, consistent with its unidimensional nature. These spectral features suggest that Bi nanolines on InAs(100) may have a strongly polarized conductivity, which makes them suitable to be exploited as nanowires in nanotechnology. The coexistence with an accumulation layer suggests an even farther functionalization.

1. Introduction

As nanoscale devices continue to shrink, components and interconnects of low dimensionality need to reach the scale of a few nanometers. As conventional lithography techniques have a natural limit of about 10–15 nm [1,2], self assembly is being considered as an attractive alternative option to fabricate nanostructures for the technology of the next generation. In this regard, one-dimensional (1D) nanolines have drawn a certain attention for their capacity to function as interconnects at the nanoscale, i.e. in nanowires [3]. Their high surface-to-volume ratio as well as their tunable electronic, thermal and transport properties give 1D nanolines a wide applicability in various fields of technology, including electronics, optoelectronics, photochemistry, and energy storage [4]. As a result, the fabrication of 1D nanolines on semiconductor surfaces was achieved via self assembly for several systems, as e.g. Pt on Ge(001), In on Si(111) and Bi on Si(100) [5–12].

Of particular interest are Bi nanolines, as they form kink-free, defect-free straight lines whose length is limited only by the size of the terraces formed on the semiconductor surface [13,14]. Their appeal for functionalization is further increased by a high stability against prolonged annealing and by the tendency to maintain a constant width [3]. Most works in the last decade have been focused on the self assembly of Bi nanolines on Si(100), which is achieved by annealing a Bi-covered Si(100) surface at around 580 °C, i.e. the Bi desorption temperature [14,15]. However, subsequent investigations on the electronic structure have emphasized the absence of energy states derived from the Bi nanolines in the vicinity of the Fermi level [16,17]. This means

* Corresponding author at: Asia Pacific Center for Theoretical Physics, Pohang, Gyeonbuk 790-784, Republic of Korea.
E-mail address: igor.dimarco@apctp.org (I. Di Marco).

https://doi.org/10.1016/j.apsusc.2022.155436
Received 2 September 2022; Received in revised form 10 October 2022; Accepted 21 October 2022
Available online 26 October 2022

that the Bi nanolines cannot conduct on their own at low bias voltages and hence are not suitable to be exploited as nanowires in prototype electronic devices.

It is natural to ask if the limitations outlined in the previous paragraph hold for other substrates as well. III–V semiconductors are important in this regard, as they have a high electron mobility and a high carrier density, making them very attractive for technology. InAs possesses a narrow, direct band gap and interesting properties for quantum transport. Moreover, the (100) and (111) surfaces of InAs host a natural charge accumulation layer [18–22], where a quasi 2D electron gas (2DEG) can form [23,24]. The curiosity of exploring these diverse, intriguing features has motivated the synthesis of uniform single-arrays of Bi nanolines on InAs(100) [25–28]. Interestingly, a variety of patterns were observed, depending on the particular conditions of growth and annealing. The most stable configuration corresponds to a (2 × 6) periodicity, which is obtained through the deposition of about 1.5 monolayers of Bi on the pristine InAs(100)-(4 × 2) surface, followed by annealing at about 520 K for 30 min to 1 h. The observed periodicity was also interpreted as an "average" reconstruction arising from patterns with smaller and larger periodicities [26]. Electronic structure calculations based on density-functional theory (DFT) can help explaining the reported experimental data. AlZaharani and Srivastava first identified that the nanolines are formed by Bi dimers on top of a monolayer of Bi dimers, which are in turn placed over the In-terminated InAs(100) surface [29]. The most favorable arrangement was found to have the Bi dimers in the nanolines parallel to those in the monolayer. Later on, Ahola-Tuomi et al. showed that a more stable configuration is obtained by creating Bi defects in the monolayer, just below the nanolines [27]. Despite the detailed structural analysis, the electronic properties of the Bi nanolines have not been addressed in detail. As we stressed above, it is crucial to identify whether the conductive character of the Bi nanolines can be associated to a detached impurity band or not. A related question is how the electronic structure of the pristine surface is going to be affected by the presence of Bi. Answering these two questions is necessary to hope to exploit these nanostructures in prototype devices.

In the present work, we investigate the electronic properties of the self-assembled Bi nanolines on top of a Bi-stabilized InAs(100) surface using angle-resolved photoemission spectroscopy (ARPES) and *ab initio* electronic structure calculations. In accordance with previous experiments, the InAs(100) surface is shown to undergo a $\zeta(4 \times 2)$ reconstruction, whereas the Bi/InAs(100) system shows a (2 × 6) symmetry. The combined experimental and theoretical analysis shows that the signature of the Bi nanolines is a strong non-dispersive resonance peak located just above the valence band maximum. This feature, in conjunction with the presence of a charge accumulation layer, suggests that the Bi nanolines on top of InAs(100) can conduct on their own and therefore may potentially act as nanowires. Most importantly, a characteristic surface resonance observed with and without Bi as well as the periodicity of the flat band demonstrate that the $\zeta(4 \times 2)$ surface reconstruction is preserved. This result emphasizes once more how crucial are the external conditions in the sample preparation and suggests that non-destructive growth can be obtained on other III–V surfaces as well.

2. Material and method

ARPES experiments were carried out at the APE beamline of the ELETTRA synchrotron radiation center, in Trieste, Italy, and at the CASSIOPÉE beamline of the SOLEIL synchrotron radiation center, in Saint-Aubin, France. All measurements were performed on undoped InAs(100) single crystals. The samples were cut along the (110) natural cleavage plane from an InAs[100] oriented surface. The In-terminated InAs(100) clean surfaces were first prepared with several cycles of Ar-ion bombardment at room temperature and then with subsequent heating to a temperature of 700 K. The low energy electron diffraction (LEED) patterns, reported in the Supplementary Material, demonstrated that we have achieved a high-quality In-terminated InAs(100)-$\zeta(4 \times 2)$ reconstructed surface, with self organized lines of In oriented along the [011] direction. Bismuth was deposited from a Knudsen cell calibrated with a quartz monitor and the sample was then annealed to 520 K after the deposition. The obtained LEED pattern, also reported in the Supplementary Material, shows a (2 × 6) reconstruction for the Bi, in agreement with the "average pattern" identified in previous literature [25–27]. In these studies, based on scanning tunneling microscopy, the largest separation between the Bi nanolines was found to be 4.3 nm [26] i.e. 10 times the distance of the surface unit cell of InAs(100)-(1 × 1). The Bi nanolines were found to be oriented along the $[0\bar{1}1]$ direction, also in agreement with previous literature. An important point to stress is that our (as well as previous) LEED data do not show a clear hexagonal pattern for the Bi monolayer below the nanolines, ruling out a bismuthene-like arrangement [30–32] and confirming the previously suggested dimerization [27,29]. Annealing at temperatures higher than 520 K causes the desorption of Bi. The ARPES measurement of the valence band were performed with linearly polarized photons of 31 eV energy, which is the value for which the resonant effect was found to be maximal. The electric field vector $\vec{E}$ was oriented along horizontal and vertical directions, i.e. in the surface plane or normal to it, respectively. Most measurements were performed with $\vec{E}$ along the horizontal direction. All ARPES measurements were performed at room temperature.

3. Calculations

To investigate the electronic structure of Bi/InAs(100) we performed first-principles calculations via DFT, as implemented in the Vienna *Ab-initio* Simulation Package (VASP) [33]. This code is based on the projected augmented wave (PAW) method [34] and has been shown to have a high accuracy with the most recent pseudopotentials [35]. Determining the formation of self-assembled nanostructures deposited on a substrate is a very complex problem, especially for patterns with a large periodicity. As discussed in the Introduction, previous works [27,29] have already clarified that the Bi nanolines form on top of a monolayer of Bi dimers, located on the substrate [27,29]. The precise distance between the Bi nanolines depends on the growing conditions and was found to range from 1.7 nm to 4.3 nm, corresponding to a periodicity of (2 × 4) to (2 × 10) [25–27]. Previous DFT studies showed that the local structural changes are minor across the patterns (2 × 6), (2 × 8) and (2 × 10), since the nanolines are already sufficiently distant to experience a negligible interaction [29]. Hence, for computational convenience, we adopt the smallest unit cell, corresponding to a (2 × 6) periodicity, which also corresponds to the average periodicity emphasized by our LEED patterns. The modeling of the Bi system on top of the In-terminated InAs(100) substrate was done using the repeated slab method [36]. The InAs(100) substrate was modeled with 11 layers of alternating In and As planes along the lattice vector $\vec{c}$ direction. The dangling bonds in the bottom As layer were passivated with fractionally charged pseudohydrogen atoms, with $Z = 0.75$. Three surface reconstructions were considered for the InAs(100) surface viz *(a)* the pristine unreconstructed surface, *(b)* the $\beta(4 \times 2)$ reconstructed surface, *(c)* the $\zeta(4 \times 2)$ reconstructed surface (see the Supplementary Material). The initial arrangement of the Bi dimers on top of the substrate depends on the reconstruction, but has to be consistent with the experimental evidence that the Bi nanolines are perpendicular to the In lines on the (4 × 2) surface of InAs(100). Finally, a vacuum region of 15 Å was added to separate periodic images along the out-of-plane z-direction. These initial configurations were fully relaxed, while the bottom four atomic layers of the substrate were kept fixed to their ideal bulk positions. The in-plane lattice constant was kept fixed to InAs bulk, being equal to 4.27 Å along [011] and $[0\bar{1}1]$ directions. The structures were considered optimized when the forces were found to be smaller than the convergence criterion of

0.01 eV/Å. The three initial configurations leading to the three relaxed structures discussed in the next sections have been described in the Supplementary Material, for sake of completeness. The wavefunctions were expanded within the plane-wave basis set with a kinetic energy cutoff of 500 eV. The generalized gradient approximation as implemented within the Perdew–Burke–Ernzerhof formalism (PBE-GGA) was the choice for exchange–correlation functional [37]. A Γ-centered k-point mesh of 5 × 3 × 1 was used to sample the Brillouin zone (BZ) of the supercell. Dipole corrections were applied within the Neugebauer and Scheffler scheme to avoid any artificial electrostatic fields arising due to the application of periodic boundary conditions [38]. As it is well documented that spin–orbit coupling (SOC) can have significant effects on the band structure for bulk Bi as well as 2D Bi surfaces [39–41], electronic structure calculations were carried out with the inclusion of SOC. For a better comparison with experiment, the band structure of the supercell was unfolded onto the BZ of InAs via the BandUP code [42,43].

4. Results

4.1. Experimental observations

We start with the description of the valence band spectra in normal emission, already presented in our previous study [44] but useful to anticipate and interpret the results obtained in ARPES. In Fig. 1, we report the spectra of the clean InAs(100)-$\zeta(4 \times 2)$ reconstructed surface (blue curve), compared to the spectra recorded after Bi deposition and annealing (red and gold curves). For the clean InAs(100) surface, i.e. the blue curve, $\vec{E}$ is aligned perpendicularly to the In lines, in order to maximize their contribution to the spectra. This experimental geometry makes it possible to emphasize the presence of a strong resonance peak at the binding energy of about 3 eV. This feature is also preserved after the Bi deposition, as demonstrated by the gold curve (measured in the same geometry). Here, the peak is sitting on a secondary electron background generated by the photo-excited electrons from the InAs substrate that are crossing the Bi layer, and thus appears even higher than in absence of Bi. Since this peak corresponds to a well-known surface state of the InAs(100)-$\zeta(4 \times 2)$ reconstructed surface [45,46], we can conclude that the latter is not destroyed by the Bi deposition. The red curve in Fig. 1, instead, corresponds to the spectrum of the system after the Bi deposition, measured for $\vec{E}$ aligned to the In lines and hence perpendicular to Bi nanolines, as shown in the inset. This configuration strongly amplifies the intensity of the Bi-derived states, labeled as "1", "2" and "3". In particular, band 1, located at a binding energy between 0.4 and 0.5 eV, exhibits a marked resonant behavior.

More detailed information on the main resonant peak is provided by the ARPES spectra and constant energy surfaces reported in Fig. 2. As in Fig. 1, the orientation of the linearly polarized electric field vector $\vec{E}$ with respect to the In lines and the Bi nanolines is shown in the small sketches, one for each pair of panels. In Fig. 2(a) and Fig. 2(d), the measurements of the clean InAs(100) surface in the experimental geometry where $\vec{E}$ is perpendicular to the In lines are reported. Fig. 2(d) illustrates that the surface states touch the gap at around 0.6 eV binding energy. The corresponding constant energy surface, in Fig. 2(a), shows the precise shape of these surface states in the 2D BZ. In Fig. 2(b) and Fig. 2(e), instead, the measurements of the clean InAs(100) surface in the experimental geometry where $\vec{E}$ is parallel to the In lines are reported. In this geometry, the resonant peak at about 3 eV binding energy, indicated by the red arrow, is much reduced, as inferred from the comparison between the panels (d) and (e). This switching from resonant to non-resonant behavior is consistent with what discussed above, for Fig. 1. In both constant energy plots, i.e. panels (a) and (b), the (4 × 2) reconstruction of the InAs(100) surface can be recognized and has been emphasized with vertical dotted lines.

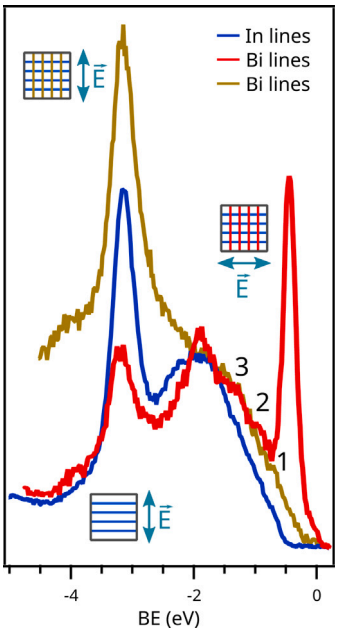

Fig. 1. Normal emission valence band spectra at the resonance photon energy (31 eV) for the clean InAs(100) surface (blue curve) and for Bi/InAs(100) (red and gold curves). The orientation of the linearly polarized electric field vector $\vec{E}$ with respect to the In lines and Bi nanolines (when present) is sketched in the inset, separately for each curve. Different experimental geometries make it possible to emphasize different contributions to the spectra. In the red curve, new bands that can be attributed to Bi are indicated and labeled as "1", "2" and "3". Similar data were reported in our previous work [44].

The same experimental geometry of Fig. 2(b) and Fig. 2(e) is then used for the ARPES measurements of the Bi/InAs(100) system, reported in Fig. 2(c) and Fig. 2(f). Fig. 2(c) shows the constant energy surface of the resonant band previously identified, located at the binding energy between 0.4 and 0.5 eV and originating from the Bi states. The band is enhanced due to the resonant behavior, obtained when $\vec{E}$ is perpendicular to the Bi nanolines, as already pointed out in the analysis of Fig. 1. The red line represents the intensity variation of the band at $k_y = 0$, while vertical lines indicate the 4× periodicity inherited from the substrate. The comparison between the ARPES spectra shown in Fig. 2(e) and Fig. 2(f) makes it possible to better characterize the Bi derived bands 1, 2 and 3. The Bi resonant peak, band 1, is a weakly dispersing flat band at a binding energy between 0.4 and 0.5 eV, located in the band gap of InAs and extending over the whole BZ. Other contributions that may be assigned to Bi appear at energies where InAs has no spectral weight as shown in the normal emission plot with a magnified energy range, on the left hand side of Fig. 2(f). Here, the green spectrum corresponds to pure InAs(100) for $\vec{E}$ perpendicular to the In lines, the blue spectrum to Bi/InAs(100) for $\vec{E}$ perpendicular to the In lines (and thus parallel to the Bi nanolines, in non-resonant conditions), and the red spectrum to Bi/InAs(100) for $\vec{E}$ parallel to the In lines (and thus perpendicular to the Bi nanolines, in resonant conditions). The labels 1, 2 and 3 have been used in analogy to Fig. 1. Despite the presence of important contributions originating from the Bi states, the InAs surface states are still clearly visible in Fig. 2(f). This not only suggests that the surface reconstruction has been preserved, but also that the interaction between Bi and the substrate is rather weak. Notably, the surface state within the band gap, indicated by a black arrow in Fig. 2(e), is unaltered by the presence of Bi, see Fig. 2(f). In addition, we observe a clear modulation of the Bi-derived flat band in the constant energy plot of Fig. 2(c), with the periodicity of the underlying In lines, i.e. one fourth of the unreconstructed BZ, as exemplified by the red intensity line. Overall, our experimental data show Bi-derived features of clear 1D nature, providing a spectral signature of the Bi nanolines.

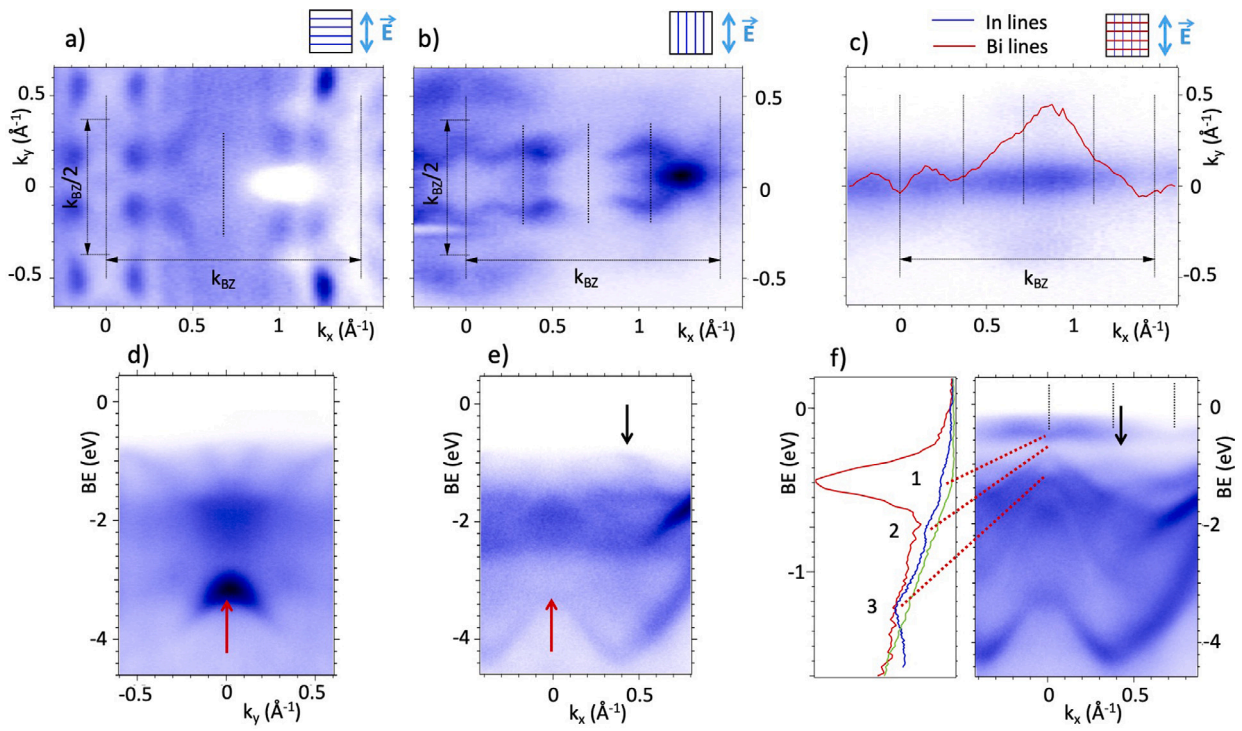

Fig. 2. ARPES measurements of the clean InAs(100)-$\zeta(4 \times 2)$ reconstructed surface are shown in panels (a), (b), (d) and (e). Panels (a) and (b) show constant energy surfaces at binding energies corresponding to the top of the valence band. The vertical lines are a guide-to-the-eye to emphasize the 2× and 4× periodicity. Above each panel, a sketch indicates the orientation of the linearly polarized electric field vector $\vec{E}$ with respect to the In lines (in blue). k_x and k_y are oriented with respect to the direction of $\vec{E}$, and hence they correspond to different directions in the 2D BZ for different geometries. Panels (d) and (e) show the corresponding ARPES spectra measured in the perpendicular direction to the In lines, i.e. along k_y in (d), with $k_x = 0$, and along k_x in (e), with $k_y = 0$. The red arrow points to the most relevant surface resonance, whose intensity is higher in panel (d), being on-resonance, and lower in panel (e), being off-resonance (see also the blue curve in Fig. 1). ARPES measurements of Bi/InAs(100) are shown in panels (c) and (f). In panel (c), the constant energy surface at a binding energy of 0.4 eV is shown, corresponding to a band originating from the Bi nanolines. As discussed for Fig. 1, this band is enhanced (on resonance) when $\vec{E}$ is perpendicular to the Bi nanolines, as indicated in the sketch above the panel. The red line represents the intensity variation of the band at $k_y = 0$, while the vertical dashed lines indicate its 4× periodicity along this direction. In panel (f), the corresponding ARPES spectrum is shown on the right hand side, as measured along the direction perpendicular to the In lines, i.e. k_x, and for $k_y = 0$. On the left hand side, the normal emission spectrum (in red) is shown, for an enhanced energy scale. For reference, the spectrum of Bi/InAs(100) for $\vec{E}$ parallel to the Bi nanolines is also shown (in blue), alongside the spectrum of the clean InAs(100) in the same geometry (in green). In the blue curve, one can identify three main features, labeled as "1", "2" and "3", as in Fig. 1. The intensity of the peak 1 is strongly enhanced in the resonant geometry for the Bi nanolines, i.e. when they are perpendicular to $\vec{E}$. The black arrows in (e) and (f) point to an InAs-surface state that is still present after the deposition of Bi, confirming that the $\zeta(4 \times 2)$ reconstruction has been preserved.

Having identified a band that can be clearly attributed to the Bi nanolines, we proceed to characterize it. In Fig. 3, the ARPES spectra for two different high symmetry directions in one fourth of the projected 2D BZ of bulk InAs are shown. The spectrum along k_x, which in this geometry corresponds to a direction that in real space is parallel to the Bi nanolines, shows the flat band having a minimum at the Γ point, then going slightly up and then decreasing again towards an energy very close to that of the Γ point, in agreement with the 4× periodicity inherited from the substrate, as discussed above. Conversely, the spectrum along k_y, which in this geometry corresponds to a direction that in real space is perpendicular to the Bi nanolines, shows the flat band having a maximum at the Γ point, then decreasing and then raising again, with a faster period than for the other direction. This is consistent with our LEED pattern (see Supplementary Material), pointing to a (2×6) symmetry for the Bi system, even in case this is only an average measurement combining patterns of different periodicities.

4.2. Morphology of Bi/InAs(100) system

The experimental data presented above raise two interesting points. First, the deposition of Bi does not seem to destroy the surface reconstruction of the substrate, which is in disagreement with the conclusions drawn in previous studies [26,27,29]. Second, the Bi nanolines contribute to the formation of an impurity-like band inside the InAs band gap, which is in sharp contrast to what was observed when Si(100) is used as a substrate. To clarify these two crucial points, we performed first-principles calculations of the entire Bi/InAs(100) system, which is a very demanding computational task.

The morphology of the Bi monolayer and the self-assembled Bi nanolines on the unreconstructed InAs(100) surface was elucidated in previous theoretical and experimental works [25,27,29]. A physical picture emerges where parallel Bi dimers arrange to form a monolayer on top of the substrate. Above the monolayer, a nanoline of pairs of Bi dimers may form. Those dimers are oriented in the same direction of the nanoline and are also parallel to the Bi dimers in the monolayer. With respect to previous literature, the following additional features have to be considered to provide a suitable model of the system probed in ARPES: 1) the (4×2) reconstruction of the InAs(100) surface is likely preserved under the Bi layers; 2) the In lines of the reconstructed surface are perpendicular to the Bi nanolines. Since the analysis of Fig. 1 and Fig. 2(f) as well as previous literature [27] suggest a weak interaction between the substrate and the Bi system, we can safely assume that different surface reconstructions are not going to induce a change in the number of dimers present in the Bi system (in other words, the Bi coverage). We will come back to this assumption before discussing the conclusions and implications of the present study. With these considerations, we construct three models corresponding to the three possible reconstructions of the InAs(100) surface that we presented in the previous subsection. For simplicity, we will refer to these three models as Bi/(2×1), Bi/$\beta(4 \times 2)$ and Bi/$\zeta(4 \times 2)$ in the rest of the paper. A short discussion on the three considered InAs(100) surface reconstructions [47–55] is provided in

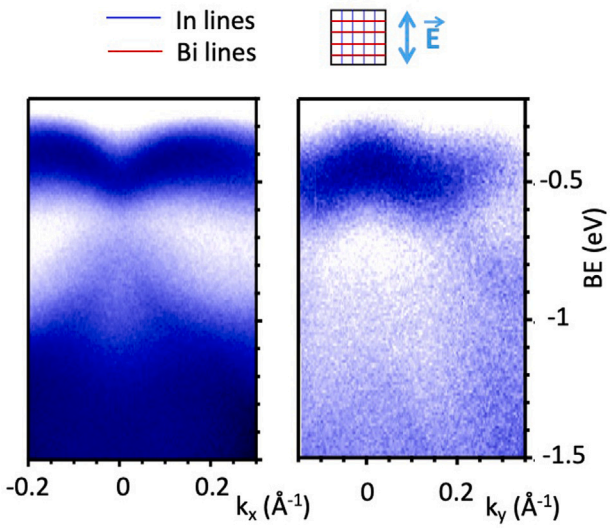

Fig. 3. ARPES spectra of Bi/InAs(100), for two different high symmetry directions in one fourth of the projected 2D BZ of bulk InAs. Above the spectra, a sketch indicates the orientation of the linearly polarized electric field vector $\vec{E}$ with respect to the In lines (in blue) and the Bi nanolines (in red). For the spectrum as a function of k_x, on the left hand side, $k_y = 0$. For the spectrum as a function of k_y, on the right hand side, $k_x = 0$. The direction of $\vec{E}$ is used as the Cartesian reference for x and y.

the Supplementary Material. The Bi/(2 × 1) model is analogous to that proposed by Ahola-Tuomi et al. [27] and requires a minimum in-plane supercell size of (2 × 6). The Bi/β(4 × 2) and Bi/ζ(4 × 2) correspond to two possible reconstruction compatible with the formation of the In lines suggested by the formation of the resonant peak at 3 eV binding energy, see Fig. 1, and requires a minimum in-plane supercell size of (4 × 6). It should be noted that the requirement that the In lines are oriented along the [011] direction while the Bi nanolines are oriented along the [0$\bar{1}$1] direction reduces the possible starting points for the structural relaxation to only a few configurations.

The optimized geometries for the three models are shown in Fig. 4. Depending on the reconstruction of the InAs(100) surface, the arrangement of Bi dimers belonging to the monolayer differs from that of the Bi dimers belonging to the nanolines. For the Bi/InAs(100) geometry, the Bi dimers in the monolayer and the nanolines are all aligned in parallel along the [0$\bar{1}$1] direction, which is in agreement with previous works [27,29]. The introduction of surface reconstruction does however affect the direction of the Bi dimerization. For the Bi/(2 × 1) geometry, it is observed that the Bi atoms of the monolayer dimerize along the [011] direction and are thus perpendicular to the Bi dimers of the nanoline. On the other hand, the Bi/ζ(4 × 2) geometry shows a mixed dimerization. The Bi atoms of the nanolines dimerize along the [011] direction perpendicular to the growth direction of the nanolines. In the monolayer, the Bi atoms far from the nanoline dimerize along the [0$\bar{1}$1] direction, while the Bi atoms beneath the nanoline dimerize along the [011] direction.

An increase in out-of-plane buckling with decreasing inter-layer separation is noted as we proceed from the most symmetric Bi/(2 × 1) system to the least symmetric Bi/ζ(4 × 2) system. The inter-layer separation between the Bi monolayer and the topmost layer of the InAs(100) surface decreases from 2.17 Å, for Bi/(2 × 1), to 1.60 Å and 1.25 Å, for respectively Bi/β(4 × 2) and Bi/ζ(4 × 2). This decrease can be attributed to the nature of the (4 × 2) reconstructed InAs(100) surface, which contains 2 atoms less than the unreconstructed one. This induces an increased interaction between the surface and the Bi monolayer, resulting in an observable buckling of the Bi layers, which leads to a reduced inter-layer separation. Furthermore, in the ζ(4 × 2) reconstructed InAs(100) surface, 4 of the 8 As atoms rise in the topmost position (see e.g. Fig. 4). Considering that the atomic radius of As, namely 1.15 Å, is smaller than that of In, namely 1.55 Å, the InAs(100)-ζ(4 × 2) surface has a more open, less closely packed geometry with several hollow sites. Consequently, the interaction between the Bi monolayer and the reconstructed surface is increased in comparison to the other systems, leading to the smallest inter-layer separation. This strong interaction, coupled with the open geometry of the surface, results in a higher degree of buckling. Despite this buckling affects the topmost layers of the InAs(100)-ζ(4 × 2) surface as well, the distortion remains a local effect and the overall geometry of the reconstruction is still preserved. This conclusion is also supported by the analysis of the electronic structure, which is provided in the next subsection.

4.3. Electronic structure of the Bi/InAs(100) surface

After having discussed three possible geometries for our sample, we can analyze their electronic structure with respect to the ARPES spectra. To this aim, it is important to unfold [42,43] the band structure of the supercells onto a BZ that is consistent with the one used to interpret the experimental data. The latter was conveniently chosen to match the unreconstructed (1 × 1) in-plane cell of the InAs(100) substrate, which has a lattice parameter ≈ 4.27 Å along the [0$\bar{1}$1] and [011] directions. The unfolded band structures are then shown in Fig. 5. The path $Y - \Gamma$ corresponds to probing along the [0$\bar{1}$1] direction, which is parallel to the Bi nanolines, i.e. k_x in the geometry of Fig. 3. The $\Gamma - X$ direction corresponds to probing along the [011] direction, which is perpendicular to the Bi nanolines, i.e. k_y in the geometry of Fig. 3.

The first feature to note is that all systems exhibit a rather well defined valence band arising from bulk InAs and reaching a maximum at about 0.5 eV below the chemical potential. Conversely, the conduction band is not so well defined, due to the overlap with the Bi states. More in detail, we note that the states that should define the conduction band minimum, at the Γ point, cross the Fermi level for both Bi/(2 × 1) and Bi/β(4 × 2). This implies that both these systems have a metallic character, while Bi/ζ(4 × 2) retains the semiconducting character observed in experiment. Although this could suggest that we should focus only on the latter, we should not forget the fact that DFT in local or semi-local approximation is well known to tend to underestimate band gaps in semiconductors in general [56,57] and

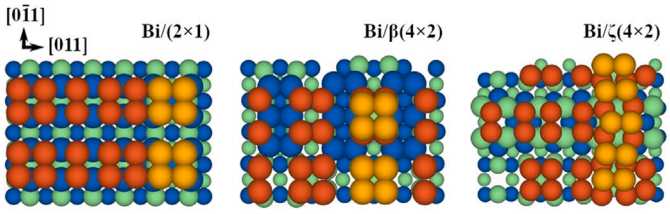

Fig. 4. Top view of the Bi/(2 × 1), Bi/β(4 × 2) and Bi/ζ(4 × 2) surfaces. Blue spheres denote the In atoms and light green spheres denote the As atoms. Bi atoms belonging to the monolayer and the nanoline are denoted by orange and yellow spheres, respectively. The size of the spheres reflects the distance from the surface. An alternative visualization of these structures is also provided in the Supplementary Material.

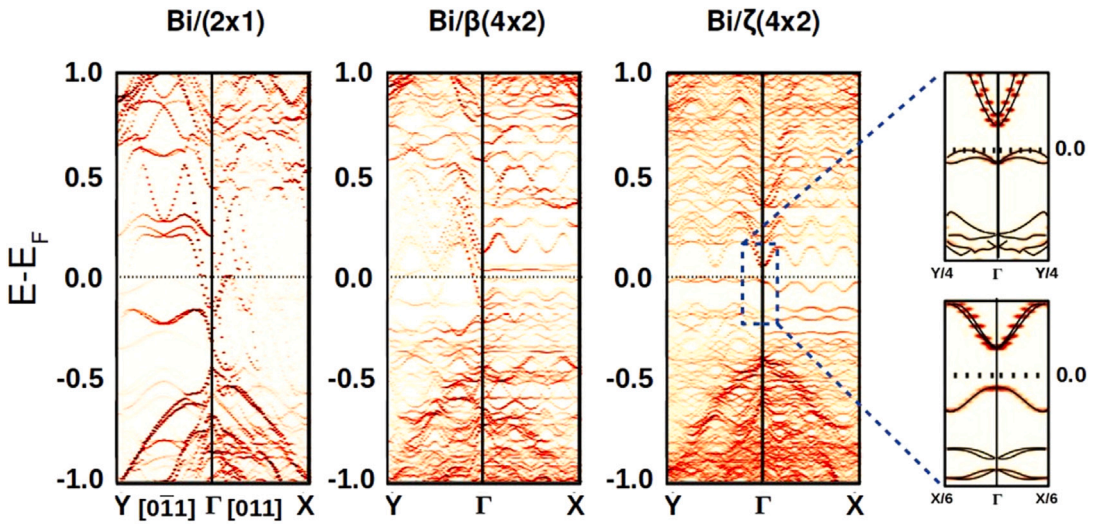

Fig. 5. The band structures of the Bi/(2 × 1), Bi/β(4 × 2) and Bi/ζ(4 × 2) surfaces unfolded onto the InAs(100) (1 × 1) cell, as obtained by DFT in GGA-PBE with SOC. Zero energy corresponds to the Fermi energy of the supercell. For a better comparison with the experimental data, two additional panels on the right hand side show the band structure of the Bi/ζ(4 × 2) geometry magnified in the most relevant energy range and along the high-symmetry paths $Y/4 - \Gamma - Y/4$ (top) and $X/6 - \Gamma - X/6$ (bottom), reflecting the expected periodicity.

for InAs in particular [22,58,59]. The second feature to focus on is whether our theoretical spectra allow us to identify the localized band corresponding to the resonant state associated to the Bi nanoline. The precise position of the band may differ between theory and experiment, due to the uncertainty in determining the chemical potential to use as a reference. This uncertainty is a consequence of the aforementioned error on the band gap, the difficulties in accounting for the accumulation layer and finally in effects beyond our model, as e.g. impurities. A better reference is the distance between the flat band and the valence band maximum, which can be estimated from Fig. 1, Fig. 2 and Fig. 3 to be around 0.5 eV. Based on these considerations, and taking into account the aforementioned uncertainties in comparing theory and experiment, we can look for the experimentally observed flat band in the region of the theoretical spectra comprised between −0.2 eV and 0.2 eV.

Fig. 5 illustrates that nearly flat states are present in all three structures, but are more pronounced in those based on the (4 × 2) reconstruction. To make sure we are able to identify the correct flat band, we have to emphasize the following key features observed from the experimental data: (1) along the $Y - \Gamma$ direction, the flat band exhibits a minimum at Γ and a maximum right close to it (see the left hand side of Fig. 3); (2) along the $Y - \Gamma$ direction, the flat band has a 4-fold modulation matching the periodicity of the underlying substrate [see panel (c) in Fig. 2]; (3) along the $\Gamma - X$ direction, the flat band exhibits a maximum at the Γ-point (see the right hand side of Fig. 3); (4) the contribution to the flat band arising from the Bi nanoline should have mainly a p_x orbital character, with the x-axis in real space being aligned along the [011] direction (conclusions derived comparing ARPES data with horizontal and vertical polarizations, data not shown). The inspection of Fig. 5 demonstrates that the only band that satisfies the first three criteria is the localized band observed just below the Fermi level in Bi/ζ(4 × 2). In particular, the third criterion leads us to exclude most of the localized bands that are visible in the spectrum. To better verify that the shape of this band matches the experimental data of Fig. 3, two magnified panels in the relevant energy range are also shown in Fig. 5, providing a direct comparison between theory and experiment. Then, we can proceed to verify if the flat band observed in Bi/ζ(4 × 2) satisfies the fourth criterion as well. To this aim, we investigate the projected density of states for the atoms composing the nanolines, reported in Fig. 6. A we can see, the p_x orbital character is dominant in the region just below the Fermi level, which is consistent with experimental data collected with different polarizations. All the previous considerations allow us to identify the localized band observed in ARPES as arising from the Bi nanolines on top of the ζ(4 × 2) reconstruction of InAs(100). In turn, this also confirms the fact that the Bi deposition does not destroy the native reconstruction of the InAs(100) surface.

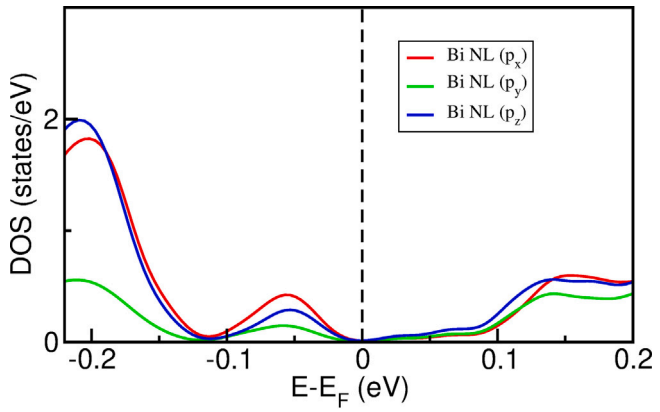

Fig. 6. The orbital contributions p_x (red), p_y (green) and p_z (blue) to the projected density of states of the atoms composing the Bi nanolines. Zero energy corresponds to the Fermi energy of the supercell.

Before moving to the conclusions, it is worth commenting on the accuracy of our theoretical modeling. The large size of the system, encompassing several layers of the substrate plus a total in-plane periodicity of (4 × 6), the uncertainty on the precise number of Bi dimers and defects, as well as the limitations of DFT in modeling semiconductors make it possible to only offer a qualitative analysis of the geometry and, thus, the electronic structure. A more precise quantitative modeling is unfortunately not accessible at the moment, but it will be interesting to address with the next generation of electronic structure codes.

5. Conclusions

We have reported the results of a joint experimental and theoretical investigation of the electronic structure of self-assembled Bi nanolines deposited on top of the InAs(100) surface. The comparison

of theoretical and experimental electronic structure demonstrates that the self-assembled Bi nanolines drive the formation of a flat band located inside the band gap, approximately 0.5 eV above the valence band maximum and 0.1 eV below the charge accumulation layer. The presence of conducting states that can be affected by a low bias voltage opens interesting perspectives for the application of this type of nanostructures as nanowires in electronic devices. Having a flat band with a one-dimensional character may also be evidence of a Luttinger liquid, albeit only future studies will be able to clarify this point. Furthermore, our analysis shows a surface resonance associated to the $\zeta(4 \times 2)$ reconstruction which persists also after the Bi deposition. This finding is contrary to the observations drawn from the previous syntheses of the Bi nanolines, where it was shown that after annealing a transition to the native unreconstructed surface is obtained [25–27]. Our findings mean that one can possibly tailor the conditions of growth and annealing to preserve a certain type of surface reconstruction, including the formation of a charge accumulation layer. The possibility of interplay between these diverse aspects is very intriguing for future nanotechnology based on self-assembly.

CRediT authorship contribution statement

Dhani Nafday: Conceptualization, Methodology, Formal analysis, Investigation, Validation, Writing – original draft, Visualization. **Christine Richter:** Conceptualization, Methodology, Resources, Supervision, Project administration, Writing – original draft, Visualization. **Olivier Heckmann:** Investigation, Validation, Writing – review & editing. **Weimin Wang:** Investigation, Validation, Writing – review & editing. **Jean-Michel Mariot:** Investigation, Validation, Writing – review & editing. **Uros Djukic:** Investigation, Validation, Writing – review & editing. **Ivana Vobornik:** Investigation, Validation, Writing – review & editing. **Patrick Lefevre:** Investigation, Validation, Writing – review & editing. **Amina Taleb-Ibrahimi:** Investigation, Validation, Writing – review & editing. **François Bertran:** Investigation, Validation, Writing – review & editing. **Julien Rault:** Investigation, Validation, Writing – review & editing. **Laurent Nicolaï:** Methodology, Investigation, Writing – review & editing. **Chin Shen Ong:** Methodology, Formal analysis, Writing – review & editing. **Patrik Thunström:** Software, Writing – review & editing. **Karol Hricovini:** Conceptualization, Methodology, Validation, Resources, Writing – original draft, Supervision, Project administration. **Ján Minár:** Conceptualization, Methodology, Validation, Writing – review & editing, Supervision, Project administration. **Igor Di Marco:** Conceptualization, Methodology, Validation, Formal analysis, Resources, Writing – original draft, Supervision, Project administration.

Declaration of competing interest

The authors declare that they have no known competing financial interests or personal relationships that could have appeared to influence the work reported in this paper.

Data availability

Data will be made available on request.

Acknowledgments

The calculations were performed on resources provided by the Swedish National Infrastructure for Computing (SNIC) at the Center for High Performance Computing (PDC) in Stockholm, Sweden, partially funded by the Swedish Research Council through Grant Agreement No. 2018-05973. Johan Hellsvik and Xin Li at PDC are acknowledged for assistance concerning technical and implementation aspects in making the code run on the clusters Beskow and Dardel. I.D.M. acknowledges support from the JRG Program at APCTP through the Science and Technology Promotion Fund and Lottery Fund of the Korean Government, as well as from the Korean Local Governments-Gyeongsangbuk-do Province and Pohang City. D.N. and I.D.M. also acknowledge financial support from the National Research Foundation of Korea (NRF), funded by the Ministry of Science and ICT (MSIT), through the Mid-Career Grant No. 2020R1A2C101217411. Ja.M. and L.N. would like to thank the CEDAMNF (Grant No. CZ.02.1.01/0.0/0.0/15_003/0000358) co-funded by the Ministry of Education, Youth and Sports of Czech Republic and the GAČR Project No. 20-18725S for funding. This publication was published with the financial support of the European Union within the Project No. CZ.02.2.69/0.0/0.0/18_054/0014627, Development of capacities and environment for boosting the international, intersectoral and interdisciplinary cooperation at UWB.

Appendix A. Supplementary data

Supplementary material related to this article can be found online at https://doi.org/10.1016/j.apsusc.2022.155436.

References

[1] A.N. Broers, Resolution limits of PMMA resist for exposure with 50 kV electrons, J. Electrochem. Soc. 128 (1) (1981) 166–170.
[2] H.G. Craighead, R. Howard, L. Jackel, P. Mankiewich, 10-nm linewidth electron beam lithography on GaAs, Appl. Phys. Lett. 42 (1) (1983) 38–40.
[3] D. Bowler, Atomic-scale nanowires: Physical and electronic structure, J. Phys.: Condens. Matter 16 (24) (2004) R721–R754.
[4] A. Machín, K. Fontánez, J.C. Arango, D. Ortiz, J. De León, S. Pinilla, V. Nicolosi, F.I. Petrescu, C. Morant, F. Márquez, One-dimensional (1D) nanostructured materials for energy applications, Materials 14 (10) (2021) 2609.
[5] J. Nogami, S.-I. Park, C. Quate, Indium-induced reconstructions of the Si(111) surface studied by scanning tunneling microscopy, Phys. Rev. B 36 (11) (1987) 6221–6224.
[6] H.W. Yeom, S. Takeda, E. Rotenberg, I. Matsuda, K. Horikoshi, J. Schaefer, C.M. Lee, S.D. Kevan, T. Ohta, T. Nagao, S. Hasegawa, Instability and charge density wave of metallic quantum chains on a silicon surface, Phys. Rev. Lett. 82 (24) (1999) 4898–4901.
[7] T. Uchihashi, U. Ramsperger, Electron conduction through quasi-one-dimensional indium wires on silicon, Appl. Phys. Lett. 80 (22) (2002) 4169–4171.
[8] O. Gurlu, O.A. Adam, H.J. Zandvliet, B. Poelsema, Self-organized, one-dimensional Pt nanowires on Ge(001), Appl. Phys. Lett. 83 (22) (2003) 4610–4612.
[9] J. Schäfer, D. Schrupp, M. Preisinger, R. Claessen, Conduction states with vanishing dimerization in Pt nanowires on Ge(001) observed with scanning tunneling microscopy, Phys. Rev. B 74 (4) (2006) 041404.
[10] M. Naitoh, H. Shimaya, S. Nishigaki, N. Oishi, F. Shoji, Scanning tunneling microscopy observation of bismuth growth on Si (100) surfaces, Surf. Sci. 377 (1997) 899–903.
[11] K. Miki, J. Owen, D. Bowler, G. Briggs, K. Sakamoto, Bismuth-induced structures on Si(001) surfaces, Surf. Sci. 421 (3) (1999) 397–418.
[12] R.V. Belosludov, A.A. Farajian, H. Mizuseki, K. Miki, Y. Kawazoe, Electronic and transport properties of bismuth nanolines for applications in molecular electronics, Phys. Rev. B 75 (11) (2007) 113411.
[13] K. Miki, D. Bowler, J. Owen, G. Briggs, K. Sakamoto, Atomically perfect bismuth lines on Si(001), Phys. Rev. B 59 (23) (1999) 14868–14871.
[14] J. Owen, K. Miki, H. Koh, H. Yeom, D. Bowler, Stress relief as the driving force for self-assembled Bi nanolines, Phys. Rev. Lett. 88 (22) (2002) 226104.
[15] M. Naitoh, H. Shimaya, S. Nishigaki, N. Oishi, F. Shoji, Bismuth-induced surface structure of Si(100) studied by scanning tunneling microscopy, Appl. Surf. Sci. 142 (1–4) (1999) 38–42.
[16] J. MacLeod, R. Miwa, G. Srivastava, A. McLean, The electronic origin of contrast reversal in bias-dependent STM images of nanolines, Surf. Sci. 576 (1–3) (2005) 116–122.
[17] J. Owen, K. Miki, D. Bowler, Interaction between electronic structure and strain in Bi nanolines on Si(001), Surf. Sci. 527 (1–3) (2003) L177–L183.
[18] L. Olsson, C. Andersson, M. Håkansson, J. Kanski, L. Ilver, U.O. Karlsson, Charge accumulation at InAs surfaces, Phys. Rev. Lett. 76 (19) (1996) 3626–3629.
[19] M. Noguchi, K. Hirakawa, T. Ikoma, Intrinsic electron accumulation layers on reconstructed clean InAs(100) surfaces, Phys. Rev. Lett. 66 (17) (1991) 2243–2246.
[20] N. Tomaszewska, L. Walczak, J. Lis, J.J. Kolodziej, Surface states and charge accumulation states on reconstructed InAs(001) surfaces, Surf. Sci. 632 (2015) 103–110.
[21] P. De Padova, C. Quaresima, P. Perfetti, R. Larciprete, R. Brochier, C. Richter, V. Ilakovac, P. Bencok, C. Teodorescu, V.Y. Aristov, R.L. Johnson, K. Hricovini, Electron accumulation layer on clean In-terminated InAs(001)(4×2)-c(8×2) surface, Surf. Sci. 482–485 (2001) 587–592.

[22] I.I. Vrubel, D. Yudin, A.A. Pervishko, On the origin of the electron accumulation layer at clean InAs(111) surfaces, Phys. Chem. Chem. Phys. 23 (8) (2021) 4811–4817.

[23] M. Morgenstern, J. Klijn, C. Meyer, M. Getzlaff, R. Adelung, R. Römer, K. Rossnagel, L. Kipp, M. Skibowski, R. Wiesendanger, Direct comparison between potential landscape and local density of states in a disordered two-dimensional electron system, Phys. Rev. Lett. 89 (13) (2002) 136806.

[24] M. Morgenstern, J. Klijn, C. Meyer, R. Wiesendanger, Real-space observation of drift states in a two-dimensional electron system at high magnetic fields, Phys. Rev. Lett. 90 (5) (2003) 056804.

[25] P. Laukkanen, M. Ahola, M. Kuzmin, R. Perälä, I. Väyrynen, J. Sadowski, Bi-induced (2×6), (2×8), and (2×4) reconstructions on the InAs(100) surface, Surf. Sci. 598 (1–3) (2005) L361–L367.

[26] M. Ahola-Tuomi, P. Laukkanen, M. Punkkinen, R. Perälä, I. Väyrynen, M. Kuzmin, K. Schulte, M. Pessa, Formation of an ordered pattern of Bi nanolines on InAs(100) by self-assembly, Appl. Phys. Lett. 92 (1) (2008) 011926.

[27] M. Ahola-Tuomi, M.P.J. Punkkinen, P. Laukkanen, M. Kuzmin, J. Lång, K. Schulte, A. Pietzsch, R. Perälä, N. Räsänen, I. Väyrynen, Properties of self-assembled Bi nanolines on InAs(100) studied by core-level and valence-band photoemission, and first-principles calculations, Phys. Rev. B 83 (24) (2011) 245401.

[28] K. Szamota-Leandersson, M. Leandersson, P. Palmgren, M. Göthelid, U.O. Karlsson, Electronic structure of bismuth terminated InAs(100), Surf. Sci. 603 (1) (2009) 190–196.

[29] A. AlZahrani, G. Srivastava, Density-functional calculations for self-assembled Bi-nanolines on the InAs(100) surface, J. Appl. Phys. 106 (5) (2009) 053713.

[30] E. Aktürk, O.Ü. Aktürk, S. Ciraci, Single and bilayer bismuthene: Stability at high temperature and mechanical and electronic properties, Phys. Rev. B 94 (1) (2016) 014115.

[31] Y. Kadioglu, S.B. Kilic, S. Demirci, O.Ü. Aktürk, E. Aktürk, S. Ciraci, Modification of electronic structure, magnetic structure, and topological phase of bismuthene by point defects, Phys. Rev. B 96 (2017) 245424.

[32] M.-Y. Liu, Y. Huang, Q.-Y. Chen, Z.-Y. Li, C. Cao, Y. He, Strain and electric field tunable electronic structure of buckled bismuthene, RSC Adv. 7 (63) (2017) 39546–39555.

[33] G. Kresse, J. Furthmüller, Efficient iterative schemes for ab initio total-energy calculations using a plane-wave basis set, Phys. Rev. B 54 (16) (1996) 11169.

[34] G. Kresse, D. Joubert, From ultrasoft pseudopotentials to the projector augmented-wave method, Phys. Rev. B 59 (3) (1999) 1758–1775.

[35] K. Lejaeghere, G. Bihlmayer, T. Björkman, P. Blaha, S. Blügel, V. Blum, D. Caliste, I.E. Castelli, S.J. Clark, A.D. Corso, S. de Gironcoli, T. Deutsch, J.K. Dewhurst, I.D. Marco, C. Draxl, M. Dułak, O. Eriksson, J.A. Flores-Livas, K.F. Garrity, L. Genovese, P. Giannozzi, M. Giantomassi, S. Goedecker, X. Gonze, O. Grånäs, E.K.U. Gross, A. Gulans, F. Gygi, D.R. Hamann, P.J. Hasnip, N.A.W. Holzwarth, D. Iuşan, D.B. Jochym, F. Jollet, D. Jones, G. Kresse, K. Koepernik, E. Küçükbenli, Y.O. Kvashnin, I.L.M. Locht, S. Lubeck, M. Marsman, N. Marzari, U. Nitzsche, L. Nordström, T. Ozaki, L. Paulatto, C.J. Pickard, W. Poelmans, M.I.J. Probert, K. Refson, M. Richter, G.-M. Rignanese, S. Saha, M. Scheffler, M. Schlipf, K. Schwarz, S. Sharma, F. Tavazza, P. Thunström, A. Tkatchenko, M. Torrent, D. Vanderbilt, M.J. van Setten, V.V. Speybroeck, J.M. Wills, J.R. Yates, G.-X. Zhang, S. Cottenier, Reproducibility in density functional theory calculations of solids, Science 351 (6280) (2016) aad3000.

[36] G.P. Srivastava, Theoretical Modelling of Semiconductor Surfaces, World Scientific, Singapore, 1999.

[37] J.P. Perdew, K. Burke, M. Ernzerhof, Generalized gradient approximation made simple, Phys. Rev. Lett. 77 (18) (1996) 3865–3868.

[38] J. Neugebauer, M. Scheffler, Adsorbate-substrate and adsorbate-adsorbate interactions of Na and K adlayers on Al(111), Phys. Rev. B 46 (24) (1992) 16067–16080.

[39] X. Gonze, J.-P. Michenaud, J.-P. Vigneron, First-principles study of As, Sb, and Bi electronic properties, Phys. Rev. B 41 (17) (1990) 11827–11836.

[40] T. Hirahara, T. Nagao, I. Matsuda, G. Bihlmayer, E. Chulkov, Y.M. Koroteev, P. Echenique, M. Saito, S. Hasegawa, Role of spin-orbit coupling and hybridization effects in the electronic structure of ultrathin Bi films, Phys. Rev. Lett. 97 (14) (2006) 146803.

[41] Y.M. Koroteev, G. Bihlmayer, J. Gayone, E.V. Chulkov, S. Blügel, P.M. Echenique, P. Hofmann, Strong spin-orbit splitting on Bi surfaces, Phys. Rev. Lett. 93 (4) (2004) 046403.

[42] P.V. Medeiros, S. Stafström, J. Björk, Effects of extrinsic and intrinsic perturbations on the electronic structure of graphene: Retaining an effective primitive cell band structure by band unfolding, Phys. Rev. B 89 (4) (2014) 041407.

[43] P.V. Medeiros, S.S. Tsirkin, S. Stafström, J. Björk, Unfolding spinor wave functions and expectation values of general operators: Introducing the unfolding-density operator, Phys. Rev. B 91 (4) (2015) 041116.

[44] O. Heckmann, M.C. Richter, J.-M. Mariot, L. Nicolaï, I. Vobornik, W. Wang, U. Djukic, K. Hricovini, Quasi 1D structures at the Bi/InAs(100) surface, AIP Conf. Proc. 1996 (1) (2018) 020017.

[45] P. De Padova, P. Perfetti, C. Quaresima, C. Richter, M. Zerrouki, O. Heckmann, V. Ilakovac, K. Hricovini, Surface states resonance on In-terminated InAs(001)(4×2)-c(8×2) clean surface, Appl. Surf. Sci. 212–213 (2003) 10–16.

[46] P. De Padova, P. Perfetti, C. Quaresima, C. Richter, O. Heckmann, M. Zerrouki, R. Johnson, K. Hricovini, New electronic surface states on In-terminated InAs(001) 4×2-c(8×2) clean surface, Surf. Sci. 532–535 (2003) 837–842.

[47] H. Yamaguchi, Y. Horikoshi, Surface structure transitions on InAs and GaAs(001) surfaces, Phys. Rev. B 51 (15) (1995) 9836–9854.

[48] M. Göthelid, Y. Garreau, M. Sauvage-Simkin, R. Pinchaux, A. Cricenti, G. Le Lay, Atomic structure of the As-rich InAs(100) β2(2×4) surface, Phys. Rev. B 59 (23) (1999) 15285–15289.

[49] V. Berkovits, N. Witkowski, Y. Borensztein, D. Paget, Effect of surface reconstruction on the low-temperature oxidation of InAs(100): Optical investigations, Phys. Rev. B 63 (12) (2001) 121314.

[50] C. Ratsch, W. Barvosa-Carter, F. Grosse, J. Owen, J. Zinck, Surface reconstructions for InAs(001) studied with density-functional theory and STM, Phys. Rev. B 62 (12) (2000) R7719–R7722.

[51] R. Miwa, G. Srivastava, Structure and electronic states of InAs(001)-(2×4) surfaces, Phys. Rev. B 62 (23) (2000) 15778.

[52] W. Schmidt, III–V compound semiconductor (001) surfaces, Appl. Phys. A 75 (1) (2002) 89–99.

[53] C. Kumpf, D. Smilgies, E. Landemark, M. Nielsen, R. Feidenhans'l, O. Bunk, J.H. Zeysing, Y. Su, R.L. Johnson, L. Cao, J. Zegenhagen, B.O. Fimland, L.D. Marks, D. Ellis, Structure of metal-rich (001) surfaces of III–V compound semiconductors, Phys. Rev. B 64 (7) (2001) 075307.

[54] P. John, T. Miller, T.-C. Chiang, InSb(100) reconstructions probed with core-level photoemission, Phys. Rev. B 39 (3) (1989) 1730–1737.

[55] S.-H. Lee, W. Moritz, M. Scheffler, GaAs(001) surface under conditions of low As pressure: Evidence for a novel surface geometry, Phys. Rev. Lett. 85 (18) (2000) 3890–3893.

[56] M. van Schilfgaarde, T. Kotani, S. Faleev, Quasiparticle self-consistent GW theory, Phys. Rev. Lett. 96 (22) (2006) 226402.

[57] O.I. Malyi, A. Zunger, False metals, real insulators, and degenerate gapped metals, Appl. Phys. Rev. 7 (4) (2020) 041310.

[58] N.N. Anua, R. Ahmed, A. Shaari, M.A. Saeed, B.U. Haq, S. Goumri-Said, Non-local exchange correlation functionals impact on the structural, electronic and optical properties of III–V arsenides, Semicond. Sci. Technol. 28 (10) (2013) 105015.

[59] M.I. Ziane, Z. Bensaad, B. Labdelli, H. Bennacer, First-principles study of structural, electronic and optical properties of III-arsenide binary GaAs and InAs, and III-nitrides binary GaN and InN: Improved density-functional-theory study, Sensors Transducers 27 (5) (2014) 374–384.